Designing Dendrite-Free Zinc Anodes for Advanced Aqueous Zinc Batteries

Junnan Hao, Xiaolong Li, Shilin Zhang, Fuhua Yang, Xiaohui Zeng, Shuai Zhang, Guyue Bo, Chunsheng Wang,* and Zaiping Guo*

Zn metal has been regarded as the most promising anode for aqueous batteries due to its high capacity, low cost, and environmental benignity. Zn anode still suffers, however, from low Coulombic efficiency due to the side reactions and dendrite growth in slightly acidic electrolytes. Here, the Zn plating/stripping mechanism is thoroughly investigated in 1 M $ZnSO_4$ electrolyte, demonstrating that the poor performance of Zn metal in mild electrolyte should be ascribed to the formation of a porous by-product ($Zn_4SO_4(OH)_6 \cdot xH_2O$) layer and serious dendrite growth. To suppress the side reactions and dendrite growth, a highly viscoelastic polyvinyl butyral film, functioning as an artificial solid/electrolyte interphase (SEI), is homogeneously deposited on the Zn surface via a simple spin-coating strategy. This dense artificial SEI film not only effectively blocks water from the Zn surface but also guides the uniform stripping/plating of Zn ions underneath the film due to its good adhesion, hydrophilicity, ionic conductivity, and mechanical strength. Consequently, this side-reaction-free and dendrite-free Zn electrode exhibits high cycling stability and enhanced Coulombic efficiency, which also contributes to enhancement of the full-cell performance when it is coupled with MnO_2 and $LiFePO_4$ cathodes.

J. Hao, X. Li, S. Zhang, F. Yang, X. Zeng, G. Bo, Prof. Z. Guo
Institute for Superconducting and Electronic Materials
Australian Institute for Innovative Materials
University of Wollongong
Wollongong, NSW 2522, Australia
E-mail: zguo@uow.edu.au
J. Hao, Prof. Z. Guo
School of Mechanical
Materials
Mechatronics & Biomedical Engineering
University of Wollongong
Wollongong, NSW 2500, Australia
S. Zhang
ARC Centre of Excellence for Electromaterials Science
Intelligent Polymer Research Institute
Australian Institute of Innovative Materials
University of Wollongong
Wollongong, NSW 2522, Australia
Prof. C. Wang
Department of Chemical and Biomolecular Engineering
University of Maryland
College Park, MD 20740, USA
E-mail: cswang@umd.edu

The ORCID identification number(s) for the author(s) of this article can be found under https://doi.org/10.1002/adfm.202001263.

1. Introduction

Aqueous rechargeable batteries, as highly promising candidates for grid-scale energy storage, have recently received great attention due to their advantages of high safety, high ionic conductivity, low cost, and environmental benignity.[1] Among these aqueous batteries, Zn metal batteries have been intensively investigated, because the Zn anode has the advantages of high theoretical capacity (gravimetric capacity of 820 mA h g^{-1} and volumetric capacity of 5855 mA h cm^{-3}), a low reduction potential (−0.76 V vs Standard Hydrogen Electrode (SHE)), and high overpotential for hydrogen evolution in aqueous media.[2]

Although aqueous Zn batteries, including the Zn–air battery and the Zn-MnO_2 battery, have achieved great progress in recent years,[3] state-of-the-art Zn batteries with alkaline electrolyte still suffer from several critical challenges, such as Zn dissolution, shape change, passivation, dendrite growth, etc.[4] Zn electrode issues are mitigated to some extent in mild electrolyte, but it is well known that dendrite growth still exists in mild Zn systems.[5] Although the dendrite growth does not result in the same hazardous situations as in organic lithium-ion or sodium-ion batteries, such as fire or even explosion,[6] it causes unceasing water/electrolyte decomposition and further degrades the lifespan of the battery.[7] To enhance the reversibility of Zn anode in neutral electrolyte, great efforts have recently been spent on the inhibition of Zn dendrite growth, including the introduction of different electrolyte additives,[8] designing porous Zn metal architectures,[9] guiding Zn backside plating,[10] employing high concentration electrolytes,[11] and building artificial inorganic layers.[7,12] Yet, the side reactions between Zn metal and mild electrolyte have often been neglected. These reactions between Zn metal and electrolyte not only dramatically reduce the Coulombic efficiency (CE) of the Zn battery, but also constantly consume the Zn anode, which leads to a limited battery lifespan. Thus, achieving an in-depth understanding of the side reactions in slightly acidic electrolyte as well as their by-products is highly desirable for further improving the CE and cycling stability of Zn batteries.

In this work, the stability has been studied of pure Zn metal electrode in 1 M $ZnSO_4$ electrolyte. The results reveal that Zn

electrode is highly unstable in slightly acidic electrolyte because it generates a loose $Zn_4SO_4(OH)_6 \cdot xH_2O$ layer. Unfortunately, this loose layer cannot effectively block the electrolyte from coming into contact with the Zn surface, so it cannot terminate the corrosion reactions by passivating the fresh Zn. In addition, Zn plating in 1 M $ZnSO_4$ electrolyte was studied in a transparent cell, demonstrating that Zn dendrites with a palm-leaf-like morphology grew on the surface of the Zn anode. After ≈260 and ≈750 h of plating/stripping at 0.5 mA cm^{-1}, the separators in the coin cells, with thicknesses of 0.24 and 0.96 mm, were pierced by Zn dendrites, leading to battery failure. To effectively inhibit the side reactions and Zn dendrite growth, a polymer film of poly(vinyl butyral) (PVB) as an artificial solid/electrolyte interphase (SEI) layer was deposited on the surface of the Zn anode via a facile spin-coating strategy. The PVB layer can effectively remove the Zn solvated water during Zn plating/stripping, significantly suppressing the side reactions and enhancing the CE. Moreover, this polymer film also exhibits strong adhesion to the Zn surface with excellent flexibility and encouraging hydrophilicity, rendering the electrolyte distribution on the Zn surface highly homogeneous, which contributes to even Zn plating/stripping underneath the artificial SEI layer, as confirmed by in situ optical microscopy. Consequently, the PVB protected Zn (PVB@Zn) electrode delivered an extended plating/stripping cycling life of 2200 h in symmetric cells at 0.5 mA cm^{-2}. To further evaluate its practical implementation, an MnO_2/PVB@Zn battery was assembled, and it showed excellent cycling stability with a capacity retention of ≈86.6% at 5 C over 1500 cycles, much higher than that of the battery

with bare Zn electrode (where the capacity retention was only 31.8%). Additionally, this artificial layer protecting the Zn anode also enhanced the CE and long-term cycling performance of a hybrid $LiFePO_4$ (LFP)/PVB@Zn cell.
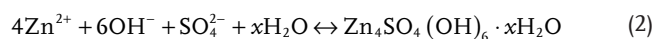
2. Results and Discussion

2.1. The Issues of Zn Anode in 1 M $ZnSO_4$ Electrolyte

To explore the side reactions between Zn metal and electrolyte, commercial Zn foil was soaked in 1 M $ZnSO_4$, as illustrated in **Figure 1**a. After 7 days, the Zn surface was seriously corroded, with the color changing from bright to gray (Figure 1b,c), indicating that Zn metal is highly unstable in 1 M $ZnSO_4$ electrolyte. The morphology of bare Zn before/after immersion in electrolyte was investigated by scanning electron microscopy (SEM). A rough and uneven surface was observed for the bare Zn foil (Figure 1d), which is mainly generated during its manufacturing process. In comparison, the Zn surface was damaged after soaking in electrolyte, and regular hexagonal flakes overgrew the whole surface (Figure 1e). Even worse, these flakes were piled up loosely on the fresh Zn surface with plenty of open space. Thus, this by-product layer could not effectively block the electrolyte and terminate the corrosion reaction, unlike the SEI layer generated on Li metal in organic electrolyte.[13] To determine the composition of the side products, X-ray powder diffraction (XRD) and Fourier transform infrared spectroscopy (FTIR) measurements were conducted.
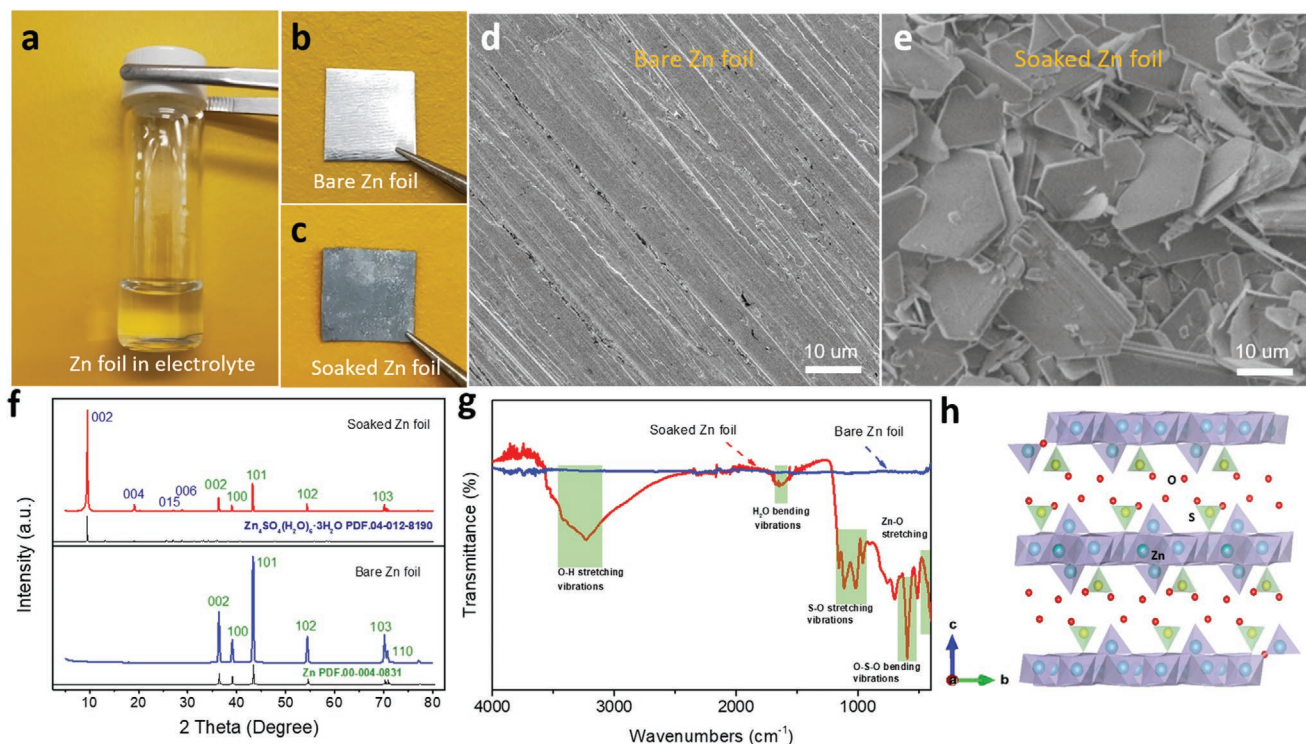
Figure 1. The stability of Zn metal in mild electrolyte. a) Zn foil soaked in 1 M $ZnSO_4$ electrolyte. b) Digital image of the bare Zn foil. c) Digital image of Zn foil after soaking in electrolyte for 7 days. SEM image of d) bare Zn foil and e) soaked Zn foil. f) XRD patterns of Zn foil before/after soaking in the electrolyte. g) FTIR spectra of Zn foil before/after soaking in the electrolyte. h) The crystal structure of $Zn_4SO_4(OH)_6 \cdot 3H_2O$ by-product.

**ADVANCED
SCIENCE NEWS**
www.advancedsciencenews.com

**ADVANCED
FUNCTIONAL
MATERIALS**
www.afm-journal.de

Figure 1f shows the XRD patterns of the Zn foil before/after soaking in electrolyte. Several new peaks clearly located at 9.5, 19.1, and 28.9 emerged after the side reactions of the Zn foil with electrolyte, corresponding to the (002), (004), and (006) planes of $Zn_4SO_4(OH)_6 \cdot 3H_2O$ (PDF.#04-012-8190), respectively. Compared with the bare Zn foil, the corroded Zn foil also showed several new conspicuous absorption peaks in its FTIR spectrum (Figure 1g). The broad absorptions at ≈3230 and ≈1630 cm^{-1} are assigned to the stretching vibrations of O—H and the bending vibrations of H_2O molecules, respectively.[14] The absorptions at ≈1160, 1100, 1000, and ≈600 cm^{-1} are attributed to the asymmetric and symmetric S—O stretching vibrations of SO_4^{2-} and the O—S—O bending vibrations of SO_4^{2-}.[15] The ≈520 cm^{-1} and ≈417 cm^{-1} peaks reflect the stretching of the Zn—O bonds, combined with librational vibrations of H_2O molecules.[16] All the absorptions on the FTIR spectrum are well matched with $Zn_4SO_4(OH)_6 \cdot xH_2O$ crystal,[17] which is also consistent with the XRD results. Figure 1h illustrates the crystal structure of $Zn_4SO_4(OH)_6 \cdot xH_2O$ with the space group $P\bar{1}$ ($a = 8.367$, $b = 8.393$, $c = 18.569$ Å; $\alpha = 90.29°$, $\beta = 89.71°$, $\gamma = 120.53°$), in which the Zn ions coordinate with oxygen ions, forming ZnO_4 tetrahedra and ZnO_6 octahedra. The Zn ion layered structure consists of the edge-sharing ZnO_6 octahedra as well as the corner-sharing ZnO_4 tetrahedra with the H_2O molecules between the layers. Overall, the side reactions of Zn electrode with electrolyte can be expressed as follows

$$Zn \leftrightarrow Zn^{2+} + 2e^- \tag{1}$$

$$4Zn^{2+} + 6OH^- + SO_4^{2-} + xH_2O \leftrightarrow Zn_4SO_4(OH)_6 \cdot xH_2O \tag{2}$$

$$2H_2O + 2e^- \leftrightarrow H_2 \uparrow + 2OH^- \tag{3}$$

Unlike Li metal in organic electrolyte, Zn metal in mild electrolyte cannot form a dense SEI film to protect the fresh Zn, since the $Zn_4SO_4(OH)_6 \cdot xH_2O$ layer is loose and porous. Moreover, this by-product layer also increases the interphase impedance between the Zn metal electrode and the electrolyte, seriously affecting the electronic/ionic diffusion at the interphase. The side reaction responsible for this and its loose by-product layer not only severely fades the CE of the Zn plating/stripping, but also shortens the cycle life of Zn batteries. Therefore, studying how to suppress the side reactions is definitely promising for further enhancing the performance of the Zn battery.

Zn plating on Zn foil in 1 M $ZnSO_4$ electrolyte was investigated using a transparent symmetrical cell at 10 mA cm^{-2} (Figure S1, Supporting Information). After 0.5 h of plating, the protrusions/dendrites grown on the Zn surface were observed with an optical microscope equipped with a digital camera, as shown in **Figure 2**a. Zn dendrites, resembling Palma leaves in their morphology (Figure 2b), grow in the perpendicular direction to the Zn metal. To study the influence of Zn dendrites on the cycling stability of Zn batteries, Zn plating/stripping in symmetric bare Zn coin-cells using separators with different thicknesses (0.24 and 0.96 mm, respectively, Figure S2, Supporting Information) was investigated at 0.5 mA cm^{-2} (Figure S3, Supporting Information). After cycling for ≈260 h, a sudden and profound polarization increase (≈4.5 V) was detected in

the symmetric Zn cell with the 0.24 mm separator, indicating battery failure.[18] On the contrary, after ≈750 h of stripping/plating, an arresting polarization was observed in the cell with the separator that was 0.96 mm thick, suggesting that the thick separator could prolong the battery life. To further understand the effects of Zn dendrites on the cycling stability, the Zn foil electrodes and separators were stripped out of the cells after 100 h, 200 h, and 300 h of cycling, as shown in Figure S4 (Supporting Information). Severe Zn corrosion with the formation of a thick resistive layer of $Zn_4SO_4(OH)_6 \cdot xH_2O$ had occurred on the Zn foil electrodes after 100 h of cycling, regardless of which separator was used. Zn corrosion also became worse with further cycling. Such serious corrosion and dendrite growth triggered battery failure by impaling the thin separator after 260 h of cycling, as evidenced by the photographs of the separators after cycling (Figure S5, Supporting Information). The results confirm that Zn dendrite growth perpendicular to the Zn foil surface is a huge potential hazard for battery failure, even in a mild electrolyte. Furthermore, the growth of Zn dendrites promotes side reactions between the Zn metal electrode and the electrolyte. This is because the fresh plated Zn deposited in the form of dendrites has a higher surface area in contact with the electrolyte, contributing to reaction of the Zn metal with the electrolyte. In turn, the side reactions also aggravate the inhomogeneity of the Zn electrode surface and the Zn^{2+} concentration polarization in the electrolyte, which provides more nuclei for deposition and a stronger driving force to form the Zn dendrites. Therefore, developing a new strategy to effectively suppress both side reactions and Zn dendrite growth in such an electrolyte is a matter of top priority to enhance the electrochemical properties of Zn-based batteries.

2.2. The Suppression of Side Reactions and Dendrite Growth by PVB Coating

Similar to Li-ion batteries, the side reactions and dendrite growth are self-enhancing in aqueous Zn-ion batteries.[19] To develop a side-reaction-free and dendrite-free Zn electrode, building an dense artificial layer on the Zn metal surface is quite promising.[12b] Theoretically, the ideal artificial layer should meet the following criteria. First, it should be water-insoluble, which helps to block the aqueous electrolyte from encountering the Zn electrode surface. Second, it should feature a high ionic conductivity and a low electronic conductivity, promoting uniform Zn^{2+} deposition underneath the artificial layer. Third, it should have strong and also flexible mechanical properties to accommodate the volumetric changes of Zn electrode during cycling. Fourth, it should have good adhesion to the Zn metal surface, so that this layer would not be detached from the Zn surface during cycling. Based on the above conditions, the PVB polymer seems appropriate. PVB is the random ternary polymer poly(vinyl butyral, vinyl alcohol, and vinyl acetate), the structure of which is shown in Figure 2c. This PVB polymer is insoluble in an aqueous solution and has been intensively applied in laminated safety glass for automobile windshields and gel electrolytes due to its strong adhesion, superior flexibility, high ionic conductivity, good mechanical stability, and favorable hydrophilic property.[20] Due to these
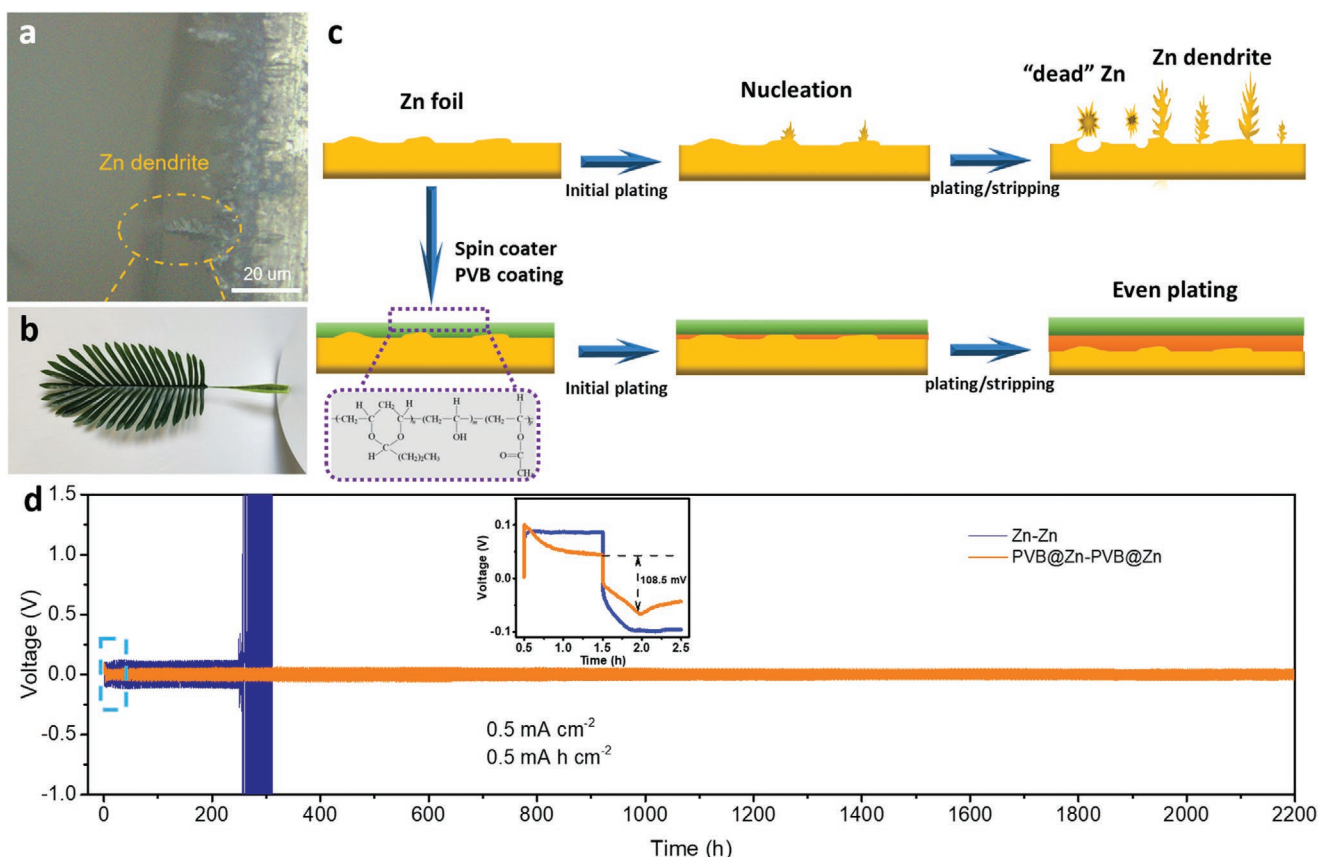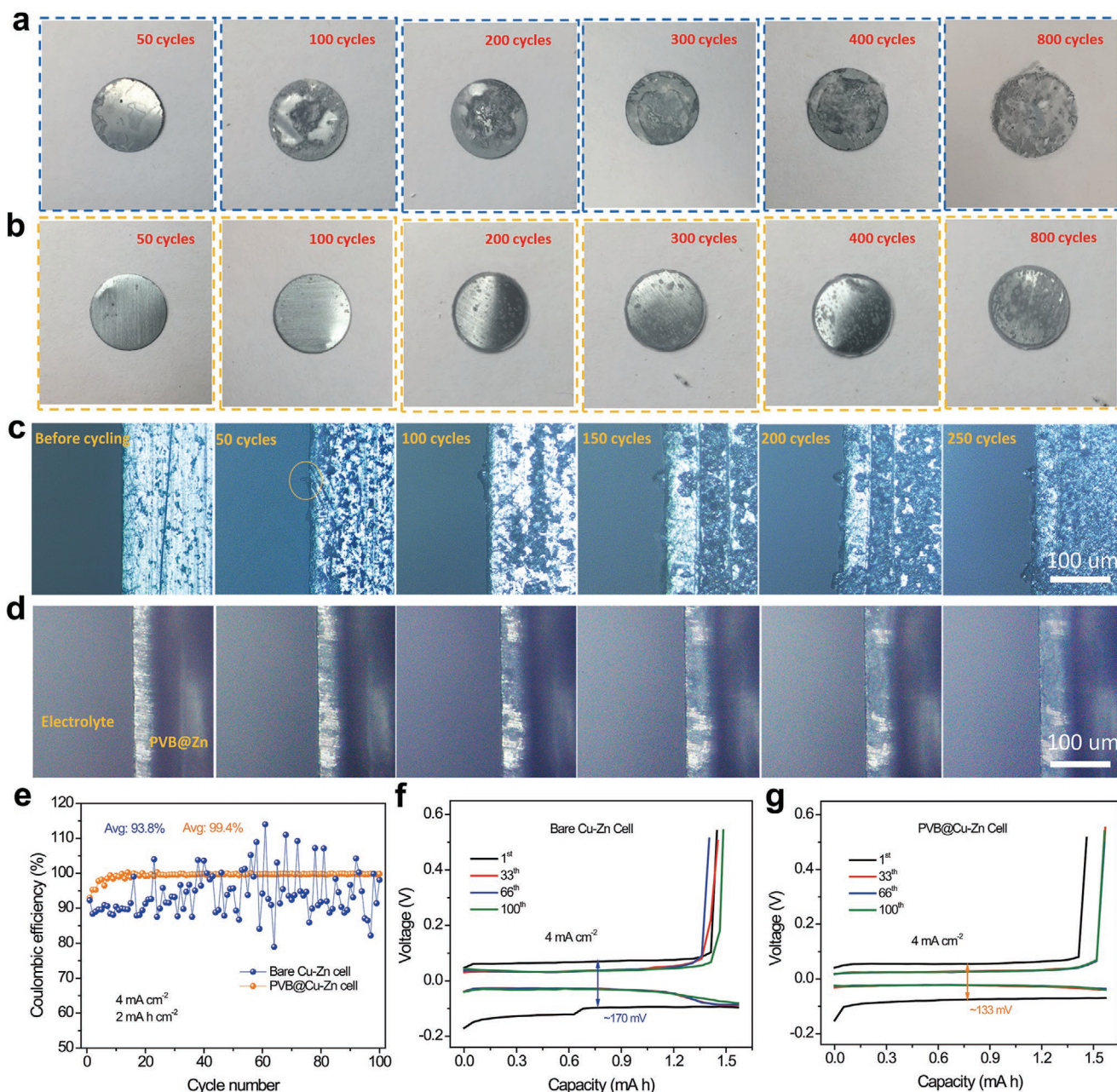
Figure 2. Zn dendrite morphology and schematic illustration of Zn plating/stripping. a) Optical microscope image of Zn dendrites on a cross section of Zn foil. b) Photograph of a palm leaf, similar to the morphology of Zn dendrites. c) Schematic illustration of morphology evolution for both the bare Zn–Zn cell and the PVB@Zn-PVB@Zn cell during repeated cycles of stripping/plating. d) Cycling stability of Zn plating/stripping in both bare Zn and PVB@Zn symmetric cells, with the inset showing the initial voltage profiles of both cells.

advantages, this PVB polymer was selected for the artificial SEI layer and deposited on the Zn metal surface using a facile spin-coating method, which not only retarded side reactions by blocking contact with the electrolyte, but also inhibited dendrite growth by promoting even Zn-ion plating/stripping.

The effectiveness of the PVB layer for enhancing the stability of PVB@Zn foil was evaluated in 1 M $ZnSO_4$ electrolyte, as illustrated in Figure S6 (Supporting Information). After 7 days, the PVB@Zn foil still maintains a bright surface without obvious corrosion, which is mainly because the electrolyte is isolated by the protective PVB film. The electrochemical performance of PVB@Zn electrode was investigated in the symmetrical PVB@Zn cells by repeated plating/stripping measurements at 0.5 mA cm^{-2} (Figure 2d). As was discussed above, the bare Zn–Zn symmetrical cell with a thin separator failed after nearly 260 h of cycling due to an internal short circuit. In strong contrast, the PVB@Zn symmetrical cell with the same thin separator displayed much smaller polarization and maintained smaller polarization curves for more than 2200 h of cycling without any internal short circuit, benefiting from the dendrite-free Zn anode. That is to say, the PVB-coating effectively inhibits the Zn dendrites and prolongs the cycle life of the Zn symmetrical cell. In addition, the polarization curves of both cells after different cycling times are compared in the inset of Figure 2d and Figure S7

(Supporting Information). At the first plating/stripping, the PVB@Zn cell shows polarization of 108.5 mV, lower than that of the bare Zn (≈200 mV) (inset of Figure 2d). Importantly, the low polarization indicates a low energy barrier for metal nucleation, which promotes a relatively uniform metal plating process.[21] After 125 cycles, a sharp increase was found in the curves for the bare Zn cell, essentially because the separator was pierced (Figure 7a, Supporting Information). In comparison, the PVB@Zn cell still features the low polarization value of 84.5 mV, which is also maintained in the following cycles, as evidenced by the value after 500 cycles (≈84.3 mV) (Figure 7b, Supporting Information).

To intuitively understand the protection of Zn foil provided by the PVB layer, Zn foil electrodes with/without PVB protection were stripped out of the symmetrical cells after different numbers of cycles. The symmetrical cells were cycled at a current density of 2 mA cm^{-2} with 10 min of intermittence, as shown in Figure S8 (Supporting Information). After 50 cycles, the digital image of PVB@Zn anode shows a bright and smooth surface (**Figure 3**a), although corrosion had occurred on the edge and surface of the bare Zn foil (Figure 3b). In the following cycles, the corrosion was aggravated, which had a serious impact on the CE and cycling stability of the Zn-based battery. In contrast, only slight corrosion at the edge of the PVB@Zn electrode was

**ADVANCED
SCIENCE NEWS**
www.advancedsciencenews.com

**ADVANCED
FUNCTIONAL
MATERIALS**
www.afm-journal.de

Figure 3. The morphology of cycled Zn anodes, optical microscopy study of Zn plating/stripping chemistry, and Coulombic efficiencies of the Zn plating/stripping. a) Digital images of Zn electrodes that were stripped out of the cells after 50, 100, 200, 300, 400, and 800 cycles. b) Digital images of PVB@Zn electrodes stripped out after the same cycle numbers. In situ optical microscope images of the front surfaces of c) Zn electrodes and d) PVB@Zn electrodes in symmetric transparent cells, along with the specified numbers of plating/stripping cycles. e) Coulombic efficiencies of the Zn plating/stripping on Cu foil with/without PVB at 4 mA cm^{-2}. Voltage profiles of the f) bare Cu foil and g) PVB coated Cu foil.

found, even after 800 cycles, which directly confirms that Zn foil was protected by PVB film during the electrochemical tests.

In order to further evaluate the inhibition of Zn dendrite growth by the PVB film, an optical microscope equipped with a digital camera (Figure S9, Supporting Information) was used for in situ monitoring of Zn plating/stripping on Zn foil in a transparent symmetrical cell. A high current density of 4 mA cm^{-2} with 10 min of intermittence was applied to repeatedly conduct the plating/stripping measurements on the transparent cells.

Figure 3c illustrates the nucleus formation as well as Zn dendrite growth at different plating/stripping cycles in the bare Zn symmetric cell. Before cycling, the Zn surface was found to be uneven, which induces the generation of nuclei. After 50 cycles, nuclei or protrusions were observed at the edges and on the surface, which is evidence of inhomogeneous Zn plating. Under further repeated plating/stripping, some nuclei evolve into Zn dendrites on the edge. Simultaneously, severe corrosion can be observed on the surface of the Zn foil, which

**ADVANCED
SCIENCE NEWS**
www.advancedsciencenews.com

**ADVANCED
FUNCTIONAL
MATERIALS**
www.afm-journal.de

distorts the electrochemical performance of Zn-based batteries. The PVB-film-protected Zn foil was also tested under the same conditions. Before cycling, the surface of the PVB@Zn foil was smooth. In the following plating/stripping process, the PVB-protected Zn electrode exhibited smooth Zn deposition with no sign of dendrites or pulverization during cycling (Figure 3d). In addition to suppressing the Zn dendrites, the impact of the PVB layer on the CE of the Zn plating/stripping behavior was also evaluated at 1 and 4 mA cm^{-2}, respectively. As illustrated in Figure S10 (Supporting Information), the PVB@Cu-Zn cell delivers a higher initial CE (83.5%) and smaller voltage hysteresis compared to the bare Cu-Zn cell (67.4%) at 1 mA cm^{-2} with a capacity of 0.5 mA h cm^{-2}. When the current was increased to 4 mA cm^{-2}, fluctuating CEs with an average value of 93.8% were obtained for the bare Cu-Zn cell (Figure 3e). In contrast, the PVB@Cu-Zn cell still presented stable CEs with the average value of 99.4%. The increased CE is mainly because the PVB film inhibits the side reactions as well as facilitating the formation of even nuclei and reversible Zn plating/stripping, as we mentioned above. Moreover, the initial voltage hysteresis in the PVB@Cu-Zn cell is ≈133 mV, which is much smaller than that in the bare Cu-Zn cell (≈170 mV) (Figure 3f,g).

### 2.3. Zn Dendrite Suppression Mechanism by PVB Coating

First, the morphology of PVB@Zn foil was studied by SEM. After spin-coating, the rough and uneven surface of Zn foil was coated by a dense and uniform PVB film (**Figure 4**a), as evidenced by the cross-sectional images with energy dispersive spectroscopy (EDS) mappings of Zn, C, and O elements (Figure 4b). PVB powders have an amorphous structure, as evidenced by the broad peak in the XRD pattern of the PVB powder (Figure 4c). FTIR spectra of this artificial PVB SEI film exhibit several characteristic peaks. The peak located at ≈3309 cm^{-1} is attributed to the symmetrical stretching vibration of O—H, as labeled in Figure 4d.[22] The absorption at ≈1726 cm^{-1} and 1129 cm^{-1} is related to the stretching vibrations of C—H and C=O bonds, respectively.[23] Then, the surface characteristics of the PVB layer (Figure 4e) were also investigated by X-ray photoelectron spectroscopy (XPS). Figure 4f presents the C 1s and O 1s spectra, which could be decomposed into several Lorentzian peaks.[24] The curve fitting results for C 1s and O 1s clearly illustrate that this artificial PVB layer has abundant oxygen-containing functional groups, which not only enhance its adhesion to the Zn metal, but also greatly boost its hydrophilicity in aqueous media.[25] The excellent adhesion between the PVB layer and the Zn foil was confirmed by rolling and twisting experiments (Figure S11, Supporting Information).

The hydrophilicity of the PVB film with respect to the electrolytes was evaluated by measuring the dynamic contact angle of Zn with/without the PVB coating at ambient temperature of 25 °C, as illustrated in **Figure 5**a,b. The initial contact angle of the bare Zn was ≈88.7°, and it remained unchanged in the following 4 min. Even after 20 min, a large contact angle of 51.8° still remained, indicating the limited hydrophilicity of the Zn
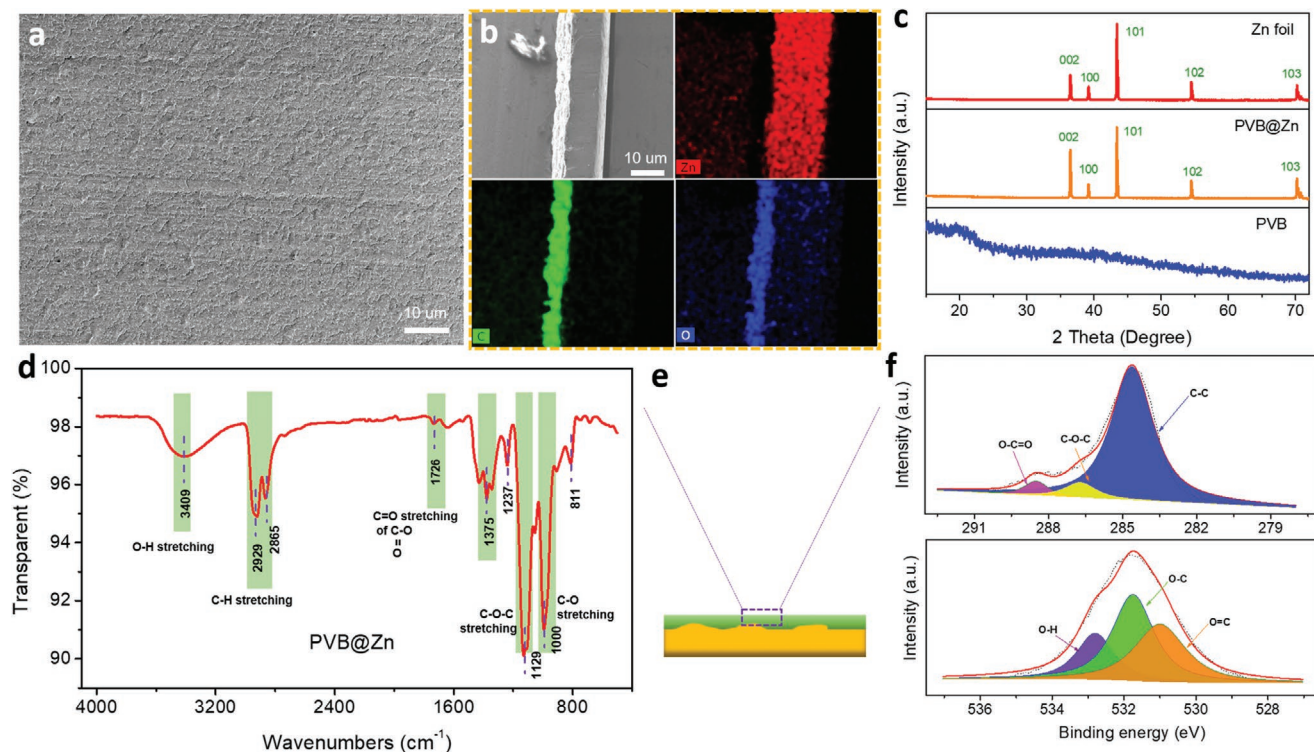
Figure 4. Characterization of bare Zn and PVB@Zn foils. a) SEM image of bare Zn foil. b) Cross-sectional SEM image of PVB@Zn foil with EDS mappings of Zn, C, and O elements, respectively. c) XRD patterns of bare Zn foil, PVB@Zn foil, and PVB. d) FTIR spectrum of PVB film on the surface of Zn foil. e) Schematic illustration of PVB@Zn foil. f) XPS analysis of PVB film, with the top panel showing the high-resolution C 1s spectrum, while the bottom panel contains the high-resolution O 1s spectrum.
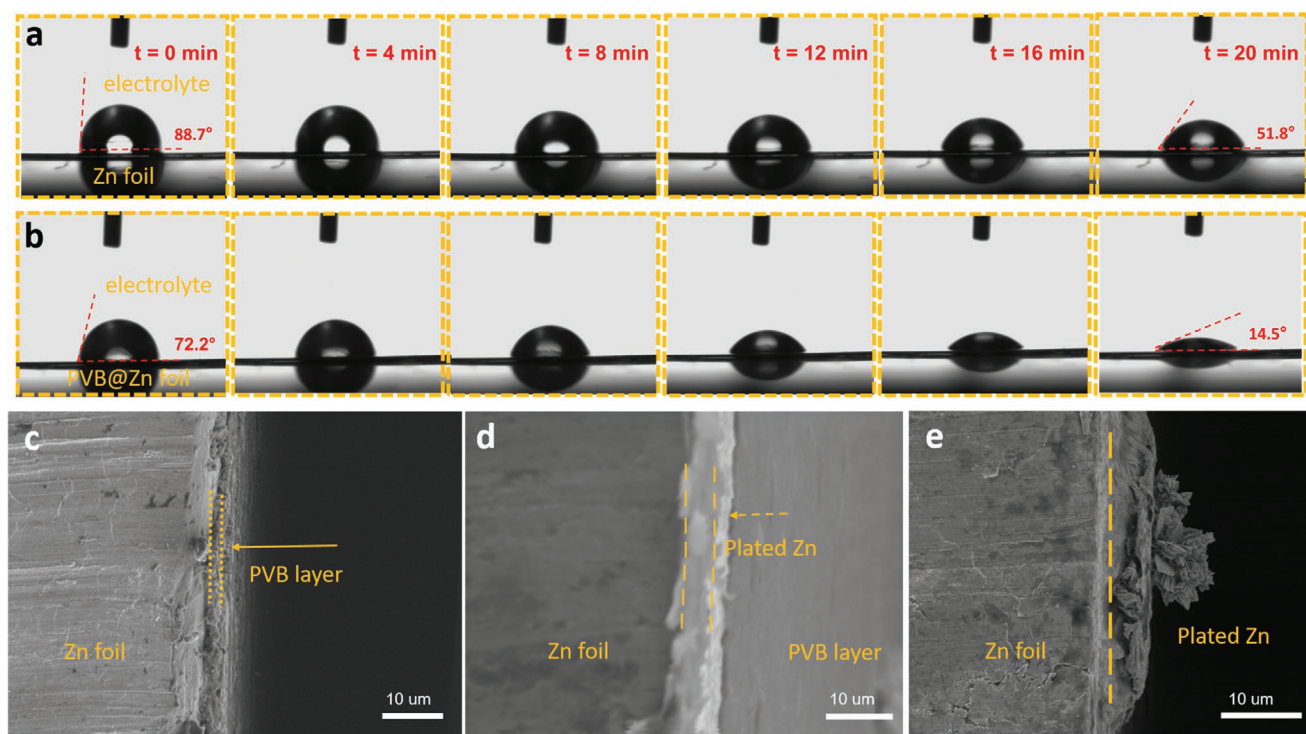
Figure 5. Hydrophilicity results and morphology of Zn foils before and after plating. a,b) In situ contact angle measurements of bare Zn and PVB@Zn foil, respectively. c–e) Cross-sectional SEM images of PVB@Zn foil, PVB@Zn foil after Zn plating, and bare Zn foil after Zn plating, respectively.

metal surface in aqueous media. In striking contrast, the initial contact angle of PVB@Zn foil was found to be 72.2°, smaller than that on the bare Zn foil. In the ensuing 20 min, it was gradually reduced to 14.5°, suggesting that the artificial PVB film dramatically enhances the hydrophilicity due to its rich polar functional groups.[26] Thermodynamically, the enhanced hydrophilicity will reduce the interfacial free energy between the Zn substrate and the electrolyte,[25] contributing to the formation of homogeneous plating and nucleation, which plays a crucial role in the final Zn plating pattern.[27] The stripping and plating of Zn with/without the PVB coating was evaluated by linear polarization experiments in 1 M $ZnSO_4$ electrolyte, as shown in Figure S12 (Supporting Information). Compared to the bare Zn electrode, the corrosion potential of the PVB coated Zn electrode increased from −1.052 to −1.010 V due to the PVB passivation layer coating. Then, SEM was employed to investigate the electrodeposition behavior of Zn-ions with/without the PVB layer (Figure 5c–e). Before plating, the cross-sectional view of the PVB@Zn foil reveals that the bare Zn surface was tightly coated by the PVB film, which had a thickness of ≈1 μm (Figure 5c). After 0.5 mA h cm^{-2} of plating (Figure S13, Supporting Information), the Zn was evenly plated under the artificial protective layer, as shown in Figure 5d.

The protective PVB layer functions as an artificial SEI and serves to prevent water from reaching the Zn surface, suppressing Zn dendrites and enhancing the CE. PVB is an electronic insulator, as verified by an electrical conductivity measurement (Figure S14, Supporting Information). The electrical resistivity was estimated as ≈2.4 × 10^5 Ω cm (the conductivity, σ = ≈4.17 × 10^{-6} S cm^{-1}, see the Supporting Information for

details). The high potential gradient in the PVB film due to the high electronic resistance of the insulating PVB film could drive Zn^{2+} diffusion through the PVB film,[28] but prevented the reduction of solvated water and anions, thus increasing the transference number. Moreover, the PVB film features good ionic conductivity (≈6.67 × 10^{-5} S cm^{-1}, Figure S15, Supporting Information), as reported elsewhere,[20,29] which facilitates the Zn^{2+} diffusion through this protective film. The transference number ($t_{Zn^{2+}}$) was further calculated to quantitatively describe the Zn^{2+} conducting ability of the PVB layer. A rather low $t_{Zn^{2+}}$ of 0.34 was obtained in the pure Zn symmetric cell (Figure S16a, Supporting Information), owing to the faster migration speed of the anions than solvated Zn^{2+}, which is consistent with a previous report.[30] $t_{Zn^{2+}}$ can be dramatically improved to 0.68, however, after introducing the PVB layer (Figure S16b, Supporting Information), because the poly(vinyl alcohol) groups in PVB provide the active sites or solvating groups for ion transfer,[31] and the dense PVB can block solvated water and anions from diffusing through the PVB. To further confirm the enhanced $t_{Zn^{2+}}$ in the PVB@Zn cells, we designed a special device to conduct in situ FTIR measurements at the electrolyte/Zn anode interface with/without the PVB film (Figure S17, Supporting Information). In the bare Zn cell, the absorption intensity of SO_4^{2-} at about 1100 cm^{-1} (due to the triply degenerate asymmetric stretching vibration) clearly decreased after Zn^{2+} plating (Figure S18, Supporting Information), demonstrating that a great many anions had moved during this period, which led to the limited $t_{Zn^{2+}}$. In strong contrast, the absorption intensity of SO_4^{2-} almost retained a similar value when Zn^{2+} plating was conducted in the PVB@Zn cells, indicating that anion

migration is much weaker at the electrolyte/Zn interface (Figure S19, Supporting Information). The high $t_{Zn^{2+}}$ also contributes to eliminating the large Zn^{2+} concentration gradient and facilitating uniform ion distribution, resulting in homogeneous Zn plating.[32]

Moreover, the dense PVB film shows excellent mechanical strength. The Young's modulus of the PVB@Zn electrode was tested using the peak force tapping (PFT) mode of an atomic force microscope (AFM; Figure S20, Supporting Information). The value of the Young's modulus of PVB film is ≈220–260 MPa, which helps to suppress the Zn dendrite growth. Hence, due to the limited electrical conductivity, good ionic conductivity, and excellent mechanical stability of the PVB film, the Zn nuclei are generated on the Zn surface instead of on the PVB film. In comparison, the Zn foil without the PVB protective film suffered from serious dendrite growth after electrodeposition (Figure 5e). These dendrites would be a potential hazard, leading to an internal short circuit of the battery.

2.4. Electrochemical Performance of LFP/PVB@Zn and MnO₂/PVB@Zn Full Cells

Hybrid LFP/PVB@Zn and MnO₂/PVB@Zn batteries were assembled to further study the impact of the PVB protective film on Zn on the performance of the full-cells. Galvanostatic charge–discharge of hybrid LFP/PVB@Zn cells at 0.5 C (where 1 C is equal to 170 mA g⁻¹,[33] **Figure 6**a) shows a flat potential plateau, corresponding to the Li⁺ ion extraction/insertion from/

into the LFP cathode,[34] which was also evidenced by ex situ XRD measurements (Figure S21, Supporting Information). Remarkably, an initial CE of 96.3% was obtained from the LFP/PVB@Zn battery (capacity of ≈153.5 mA h g⁻¹), higher than that of the battery with bare Zn electrode (an initial CE of 93.1% with a capacity of ≈149.2 mA h g⁻¹). Figure S22 (Supporting Information) shows the rate capability of LFP/Zn batteries with/without the PVB protective film. Only the capacity of 32.1 mA h g⁻¹, representing capacity retention of ≈21.5% (compared to 0.5 C), was retained in the LFP/Zn battery when the current rate was increased to 20 C. In comparison, a high capacity of 76.9 mA h g⁻¹ was still obtainable in the LFP/PVB@Zn battery at the same current rate. After 500 cycles at 5 C, the LFP/PVB@Zn battery still delivered a reversible discharge capacity of 108.4 mA h g⁻¹ and maintained a high capacity retention of 87.6%, with only 0.025% capacity fading per cycle (Figure 6b), which is much higher than that of the LFP/Zn battery with capacity retention of only 60% after 500 cycles. The morphology of Zn anodes after 500 cycles was studied by SEM. The bare Zn electrode shows serious corrosion and dendrite growth (Figure S23, Supporting Information), which is likely to be the main reason for its poor CE and limited cycling stability.[35] The PVB@Zn electrode is still even and smooth, however, and no serious corrosion or dendrites can be found (Figure S24, Supporting Information). Furthermore, the electrochemical performance of the LFP/PVB@Zn battery was also compared with other hybrid Zn-based batteries, as illustrated in Figure S25 (Supporting Information). It shows that our LFP/PVB@Zn battery is superior to other hybrid Zn-based batteries. To further
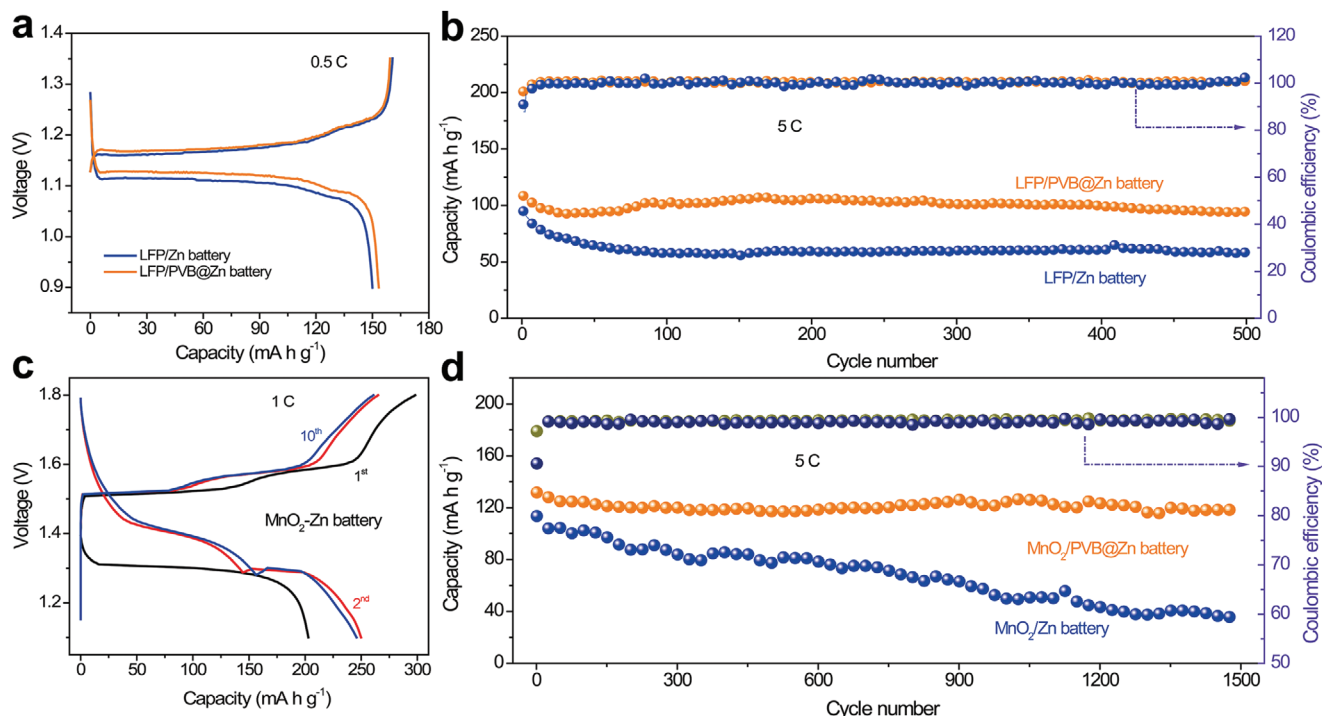
Figure 6. Electrochemical performance of Zn-based full cells. a) The first cycle charge–discharge profiles of LFP/Zn and LFP/PVB@Zn batteries at the current rate of 0.5 C. b) Long-term cycling stability of both batteries at 5 C with the corresponding CEs. c) Charge–discharge profiles of MnO₂/Zn batteries in electrolyte composed of 1 M ZnSO₄ and 0.1 M MnSO₄ solution at the rate of 1 C. d) Long-term cycling stability of MnO₂/Zn and MnO₂/PVB@Zn batteries at 5 C with the corresponding CEs.

demonstrate the versatility of our PVB SEI film on Zn anode, $MnO_2/PVB@Zn$ batteries were assembled as well, as the MnO_2/Zn battery is one of the most commonly used systems in mild aqueous electrolyte.[36] The MnO_2 was in situ synthesized on a carbon cloth by a chronoamperometric electrodeposition process, and its nanoflower morphology was characterized by SEM (Figure S26, Supporting Information). $MnO_2/PVB@Zn$ batteries were tested in an electrolyte composed of 1 M $ZnSO_4$ and 0.1 M $MnSO_4$, in which $MnSO_4$ serves as an electrolyte additive to suppress the Mn^{2+} dissolution from the cathode material. The typical charge–discharge curves of MnO_2/Zn battery at 1 C are presented in Figure 6c. Our PVB coated Zn anode helps to enhance the CE and cycling stability of the MnO_2/Zn system, as shown in Figure 6d. After 1500 cycles, the capacity retention of the $MnO_2/PVB@Zn$ battery is ≈86.6%, much higher than that of the MnO_2/Zn battery (31.8%).

3. Conclusion

In this work, the Zn surface chemistry in slightly acidic electrolyte as well as the influence of Zn dendrite growth on the electrochemical performance of Zn-based batteries was comprehensively investigated. The results reveal that Zn metal shows poor thermodynamic stability even in mild electrolyte. A by-product layer of $Zn_4SO_4(OH)_6 \cdot xH_2O$ was generated at the interphase between the Zn surface and the electrolyte, although it could not block the electrolyte due to its loose structure. In addition, Zn dendrites that formed on the bare Zn electrode would pierce the thin separator (0.24 mm) and generate an internal short circuit after prolonged plating/stripping. Although a thick separator (0.96 mm) extended the cycle life of the symmetric Zn cell, it could not fundamentally address the issues caused by the Zn dendrites. To effectively suppress the side reactions and Zn dendrite growth, an even and dense PVB SEI film was deposited on the surface of the Zn metal using the spin-coating method. Benefiting from the abundant polar functional groups of the PVB chains, this insulating polymer shows good hydrophilicity and ionic conductivity, inhibiting the side reactions and Zn dendrite growth. The side-reaction-free and dendrite-free PVB@Zn anode facilitated repeated plating/stripping over 2200 h in the symmetrical Zn cell, much longer than for the bare Zn cells. Importantly, both the commonly used MnO_2 system and the hybrid LFP system displayed higher initial CE and longer lifespan when coupled with PVB@Zn anode compared to the batteries with bare Zn anode. Our findings can help to elucidate the side reactions between Zn metal electrode and mild electrolyte, as well as Zn dendrite growth. We provide a simple and inexpensive strategy to manipulate the Zn electrodeposition behavior from dendritic to nondendritic, which paves the way to rejuvenated prospects for Zn-based batteries in large-scale applications.

Supporting Information

Supporting Information is available from the Wiley Online Library or from the author.

Conflict of Interest

The authors declare no conflict of interest.

Author Contributions

J.H. performed the experiments and wrote the manuscript. X.L. and S.Z. helped to conduct the SEM measurements. F.Y. and X.Z. analysed the electrochemical data. S.Z. performed the dynamic contact angle tests. G.B. conducted the AFM measurements. C.W. and Z.G. supervised the overall research. All the authors discussed the results and commented on the manuscript.

Keywords

[1] a) H. Kim, J. Hong, K. Y. Park, H. Kim, S. W. Kim, K. Kang, *Chem. Rev.* **2014**, *114*, 11788; b) J. Y. Luo, W. J. Cui, P. He, Y. Y. Xia, *Nat. Chem.* **2010**, *2*, 760; c) L. Suo, O. Borodin, T. Gao, M. Olguin, J. Ho, X. Fan, C. Luo, C. Wang, K. Xu, *Science* **2015**, *350*, 938; d) D. Chao, H. J. Fan, *Chem* **2019**, *5*, 1359.

[2] a) J. Huang, Z. Guo, Y. Ma, D. Bin, Y. Wang, Y. Xia, *Small Methods* **2019**, *3*, 1800272; b) G. Fang, J. Zhou, A. Pan, S. Liang, *ACS Energy Lett.* **2018**, *3*, 2480; c) Y. Li, M. Gong, Y. Liang, J. Feng, J. E. Kim, H. Wang, G. Hong, B. Zhang, H. Dai, *Nat. Commun.* **2013**, *4*, 1805; d) D. Chao, C. Zhu, M. Song, P. Liang, X. Zhang, N. H. Tiep, H. Zhao, J. Wang, R. Wang, H. Zhang, *Adv. Mater.* **2018**, *30*, 1803181.

[3] a) M. Song, H. Tan, D. Chao, H. J. Fan, *Adv. Funct. Mater.* **2018**, *28*, 1802564; b) W. Sun, F. Wang, S. Hou, C. Yang, X. Fan, Z. Ma, T. Gao, F. Han, R. Hu, M. Zhu, *J. Am. Chem. Soc.* **2017**, *139*, 9775; c) F. Wan, L. Zhang, X. Dai, X. Wang, Z. Niu, J. Chen, *Nat. Commun.* **2018**, *9*, 1656.

[4] a) X. Zeng, J. Hao, Z. Wang, J. Mao, Z. Guo, *Energy Storage Mater.* **2019**, *20*, 410; b) J. Fu, Z. P. Cano, M. G. Park, A. Yu, M. Fowler, Z. Chen, *Adv. Mater.* **2017**, *29*, 1604685.

[5] J. Zhao, J. Zhang, W. Yang, B. Chen, Z. Zhao, H. Qiu, S. Dong, X. Zhou, G. Cui, L. Chen, *Nano Energy* **2019**, *57*, 625.

[6] a) Q. Li, S. Zhu, Y. Lu, *Adv. Funct. Mater.* **2017**, *27*, 1606422; b) W. Luo, Y. Gong, Y. Zhu, Y. Li, Y. Yao, Y. Zhang, K. Fu, G. Pastel, C. F. Lin, Y. Mo, *Adv. Mater.* **2017**, *29*, 1606042.

[7] L. Kang, M. Cui, F. Jiang, Y. Gao, H. Luo, J. Liu, W. Liang, C. Zhi, *Adv. Energy Mater.* **2018**, *8*, 1801090.

[8] a) S. J. Banik, R. Akolkar, *Electrochim. Acta* **2015**, *179*, 475; b) S. J. Banik, R. Akolkar, *J. Electrochem. Soc.* **2013**, *160*, D519;

**ADVANCED
SCIENCE NEWS**

www.advancedsciencenews.com

**ADVANCED
FUNCTIONAL
MATERIALS**

www.afm-journal.de

c) K. E. Sun, T. K. Hoang, T. N. L. Doan, Y. Yu, X. Zhu, Y. Tian, P. Chen, *ACS Appl. Mater. Interfaces* **2017**, *9*, 9681; d) Q. Zhang, J. Luan, L. Fu, S. Wu, Y. Tang, X. Ji, H. Wang, *Angew. Chem., Int. Ed.* **2019**, *58*, 15841.

[9] M. Chamoun, B. J. Hertzberg, T. Gupta, D. Davies, S. Bhadra, B. Van Tassell, C. Erdonmez, D. A. Steingart, *NPG Asia Mater.*. **2015**, *7*, e178.

[10] S. Higashi, S. W. Lee, J. S. Lee, K. Takechi, Y. Cui, *Nat. Commun.* **2016**, *7*, 11801.

[11] a) C. Zhang, J. Holoubek, X. Wu, A. Daniyar, L. Zhu, C. Chen, D. P. Leonard, I. A. Rodriguez-Perez, J. X. Jiang, C. Fang, X. Ji, *Chem. Commun.* **2018**, *54*, 14097; b) F. Wang, O. Borodin, T. Gao, X. Fan, W. Sun, F. Han, A. Faraone, J. A. Dura, K. Xu, C. Wang, *Nat. Mater.* **2018**, *17*, 543.

[12] a) K. Zhao, C. Wang, Y. Yu, M. Yan, Q. Wei, P. He, Y. Dong, Z. Zhang, X. Wang, L. Mai, *Adv. Mater. Interfaces* **2018**, *5*, 1800848; b) B. Tang, L. Shan, S. Liang, J. Zhou, *Energy Environ. Sci.* **2019**, *12*, 3288.

[13] J. Qian, B. D. Adams, J. Zheng, W. Xu, W. A. Henderson, J. Wang, M. E. Bowden, S. Xu, J. Hu, J. G. Zhang, *Adv. Funct. Mater.* **2016**, *26*, 7094.

[14] M. Grechko, T. Hasegawa, F. D'Angelo, H. Ito, D. Turchinovich, Y. Nagata, M. Bonn, *Nat. Commun.* **2018**, *9*, 885.

[15] X. Guo, H. S. Xiao, F. Wang, Y. H. Zhang, *J. Phys. Chem. A* **2010**, *114*, 6480.

[16] M. Faisal, A. A. Ismail, A. A. Ibrahim, H. Bouzid, S. A. Al-Sayari, *Chem. Eng. J.* **2013**, *229*, 225.

[17] N. Chukanov, R. Rastsvetaeva, S. Aksenov, I. Pekov, D. Belakovskiy, G. Blass, G. Möhn, *Geol. Ore Deposits* **2013**, *55*, 663.

[18] C. Lan, C. Lee, T. Chin, *Electrochim. Acta* **2007**, *52*, 5407.

[19] a) N. W. Li, Y. X. Yin, C. P. Yang, Y. G. Guo, *Adv. Mater.* **2016**, *28*, 1853; b) H. Li, D. Chao, B. Chen, X. Chen, C. Chuah, Y. Tang, Y. Jiao, M. Jaroniec, S. Z. Qiao, *J. Am. Chem. Soc.* **2020**, *142*, 2012; c) H. Gao, F. Yang, Y. Zheng, Q. Zhang, J. Hao, S. Zhang, H. Zheng, J. Chen, H. Liu, Z. Guo, *ACS Appl. Mater. Interfaces* **2019**, *11*, 5373.

[20] Y. Bai, Y. Chen, Q. Wang, T. Wang, *J. Mater. Chem. A* **2014**, *2*, 9169.

[21] J. Xie, J. Wang, H. R. Lee, K. Yan, Y. Li, F. Shi, W. Huang, A. Pei, G. Chen, R. Subbaraman, *Sci. Adv.* **2018**, *4*, eaat5168.

[22] P. Thomas, J. P. Guerbois, G. Russell, B. Briscoe, *J. Therm. Anal. Calorim.* **2001**, *64*, 501.

[23] L. J. Chen, J. D. Liao, S. J. Lin, Y. J. Chuang, Y. S. Fu, *Polymer* **2009**, *50*, 3516.

[24] B. Erdem, R. A. Hunsicker, G. W. Simmons, E. D. Sudol, V. L. Dimonie, M. S. El-Aasser, *Langmuir* **2001**, *17*, 2664.

[25] D. Briggs, *J. Adhes.* **1982**, *13*, 287.

[26] a) T. Meng, F. Yi, H. Cheng, J. Hao, D. Shu, S. Zhao, C. He, X. Song, F. Zhang, *ACS Appl. Mater. Interfaces* **2017**, *9*, 42883; b) J. Hao, T. Meng, D. Shu, X. Song, H. Cheng, B. Li, X. Zhou, F. Zhang, Z. Li, C. He, *J. Colloid Interface Sci.* **2019**, *537*, 57.

[27] Z. Zhao, J. Zhao, Z. Hu, J. Li, J. Li, Y. Zhang, C. Wang, G. Cui, *Energy Environ. Sci.* **2019**, *12*, 1938.

[28] X. Liang, Q. Pang, I. R. Kochetkov, M. S. Sempere, H. Huang, X. Sun, L. F. Nazar, *Nat. Energy* **2017**, *2*, 17119.

[29] a) F. Lian, Y. Wen, Y. Ren, H. Guan, *J. Membr. Sci.* **2014**, *456*, 42; b) K. F. Chen, C. H. Liu, H. K. Huang, C. H. Tsai, F. R. Chen, *Int. J. Electrochem. Sci.* **2013**, *8*, 3524.

[30] J. L. Dye, M. P. Faber, D. J. Karl, *J. Am. Chem. Soc.* **1960**, *82*, 314.

[31] S. Gopal, S. Agnihotry, V. Gupta, *Sol. Energy Mater. Sol. Cells* **1996**, *44*, 237.

[32] R. Xu, Y. Xiao, R. Zhang, X. B. Cheng, C. Z. Zhao, X. Q. Zhang, C. Yan, Q. Zhang, J. Q. Huang, *Adv. Mater.* **2019**, *31*, 1808392.

[33] a) G. Armstrong, A. R. Armstrong, P. G. Bruce, P. Reale, B. Scrosati, *Adv. Mater.* **2006**, *18*, 2597; b) J. Hao, F. Yang, S. Zhang, H. He, G. Xia, Y. Liu, C. Didier, T. Liu, W. K. Pang, V. K. Peterson, *Proc. Natl. Acad. Sci. USA* **2020**, *117*, 2815.

[34] J. Hao, J. Long, B. Li, X. Li, S. Zhang, F. Yang, X. Zeng, Z. Yang, W. K. Pang, Z. Guo, *Adv. Funct. Mater.* **2019**, *29*, 1903605.

[35] J. S. Lee, S. Tai Kim, R. Cao, N. S. Choi, M. Liu, K. T. Lee, J. Cho, *Adv. Energy Mater.* **2011**, *1*, 34.

[36] D. Chao, W. Zhou, C. Ye, Q. Zhang, Y. Chen, L. Gu, K. Davey, S. Z. Qiao, *Angew. Chem., Int. Ed.* **2019**, *58*, 7823.

2001263 (10 of 10)